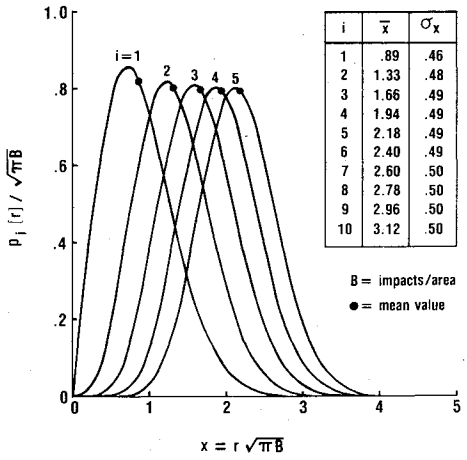

i	$\bar{x}$	σ_x
1	.89	.46
2	1.33	.48
3	1.66	.49
4	1.94	.49
5	2.18	.49
6	2.40	.49
7	2.60	.50
8	2.78	.50
9	2.96	.50
10	3.12	.50

Fig. 1 Probability density that the *i*th crater is at distance *r*.

Conclusions

Damage due to a typical impact on a surface depends on the previous state of the surface. This Note gives probability density relations for the distance to the center of the nearest damage area, the next nearest, etc. in terms of the mean number of impacts per unit area at any time. These results can be used to update probabilistic damage state specification models which involve the location of damage areas due to previous impacts.

Reference

[1] Davenport, W. B. Jr. and Root, W.L., *Random Signals and Noise*, McGraw Hill, N.Y., 1958, pp. 115-119.

Flight-Test Base Pressure Measurements in Turbulent Flow

Bruce M. Bulmer*
Sandia Laboratories, Albuquerque, N. Mex.

Nomenclature

A_B	= base area
C_{Db}	= base drag coefficient
Cp_b	= base pressure coefficient
M	= Mach number
$\dot{m}$	= total heatshield ablation (mass addition) rate
$\dot{m}/\rho_\infty V_\infty A_B$	= mass addition parameter
p	= static pressure
R	= base radial coordinate
R_B	= base radius
R_N	= nose radius
R_N/R_B	= bluntness ratio
V	= velocity
γ	= ratio of specific heats
θ_c	= cone half-angle
ρ	= static density

Subscripts

b	= base condition
c	= local (boundary-layer edge) condition on cone immediately preceding base
∞	= freestream condition

Presented at the Open Forum Session, AIAA 11th Thermophysics Conference, San Diego, Calif., July 14-16, 1976 (no preprint). Submitted July 27, 1976; revision received Sept. 7, 1976. This work was supported jointly by the U.S. Energy Research and Development Administration and the USAF Space and Missile Systems Organization.

Index categories: Boundary Layers and Convective Heat Transfer-Turbulent; Jets, Wakes, and Viscid-Inviscid Flow Interactions; Entry Vehicle Testing.

*Member Technical Staff, Aerothermodynamics Division. Member AIAA.

Introduction

DETERMINATION of the recirculating base-flow properties in the near wake of a slender cone is important in several re-entry applications. For example, the static pressures that characterize the base-flow region are required for base drag predictions[1] and serve as a necessary boundary condition in base heating calculations.[2]

This Note presents flight-test base pressure measurements for four relatively sharp, slender re-entry vehicles (RVs). The data encompass the hypersonic, supersonic, and subsonic flow regimes ($M_\infty = 0.5$-15) and are correlated to provide an empirical prediction capability for vehicles characterized by very low heatshield ablation rates in turbulent flow (mass addition parameter $\dot{m}/\rho_\infty V_\infty A_B < 0.001$).

Base Pressure Measurements

RV Configurations

The external shapes of the four RVs were nearly identical 9° half-angle spherically blunted cones. Flights 1 and 2 were 5% blunt ($R_N/R_B = 0.05$), whereas Flights 3 and 4 were 6% blunt. Base geometry was flat for all vehicles. The ablative heatshields utilized in these tests are characterized by very low ablation rates ($\dot{m}/\rho_\infty V_\infty A_B < 0.001$) in turbulent boundary-layer flow conditions.

Instrumentation

Base pressure instrumentation incorporated two sensors for each vehicle installed at two radial positions ($R/R_B = 0.1$ and 0.8) on the base cover. Statham unbonded strain-gage type transducers were used for all tests. These were designed specifically for data acquisition in the turbulent-flow regime and were sized as either 0-68.9 or 0-103 kN/m^2 abs (0-10 or 0-15 psia) full-scale range, depending on the trajectory conditions encountered by a particular vehicle. Data were telemetered at a commutated rate of 15 samples/sec.

Each transducer was isolated from heat, vibration, and shock by mounting on a short section of soft rubber tubing, which in turn was attached to the pressure port fitting in the base cover. This provided a very short pneumatic system (tube length/port diameter ratio < 12) between the sensor and pressure port and effectively eliminated any pressure time lag.

Data Presentation

Figure 1 illustrates representative base pressure measurements as a function of flight time/decreasing altitude. Mach number regimes are identified that reveal the behavior of base pressure in various flow environments. Abrupt changes in p_b observed near $M_\infty = 4$ and $M_\infty = 1$ typify the present data. Note that this particular vehicle (Flight 2) was in subsonic flow ($M_\infty > 0.5$) during the terminal portion of re-entry.

A composite comparison of all measurements is presented in Fig. 2 in terms of the base pressure ratio and freestream Mach number (M_∞ and p_∞ were determined from postflight reconstructed trajectories that incorporated the telemetered axial accelerations and the measured ambient atmospheric conditions). These results provide a continuous variation of base pressure with Mach number throughout the range $M_\infty = 0.5$-15 and include only those data that exceed 5% of the full-scale sensor output in fully developed turbulent boundary-layer flow (established by extensive onboard thermal and dynamic motion instrumentation). Corresponding freestream Reynolds numbers (referenced to vehicle length) varied from approximately 20 million at the lowest Mach numbers to a

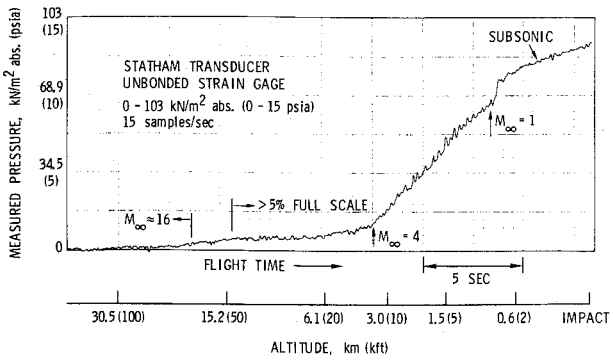

Fig. 1 Typical base pressure data trace (Flight 2, $R/R_B = 0.8$).

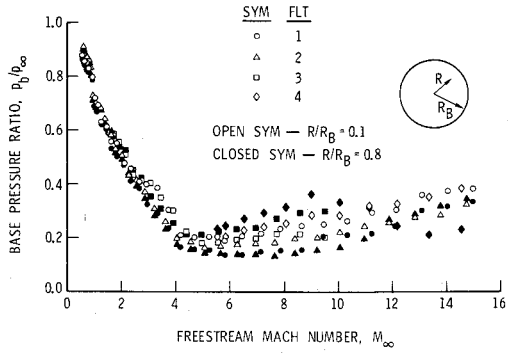

Fig. 2 Base pressure measurements in turbulent flow.

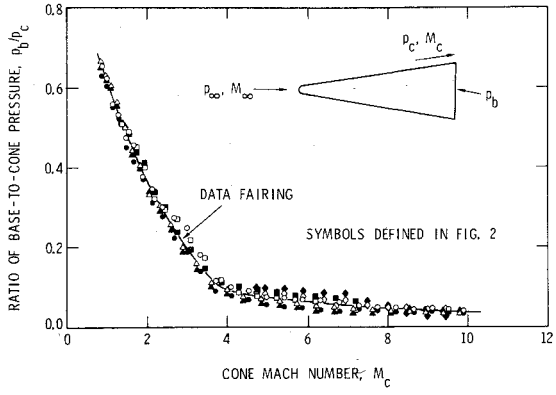

Fig. 3 Correlation of base pressure data.

maximum of 170 million in hypersonic flow. For the data presented, the angle of attack was less than 0.5°.

The flight data (Fig. 2) exhibit an increase in p_b/p_∞ with increasing M_∞ in the hypersonic regime.[3,4] Results for the centerline ($R/R_B = 0.1$) display a high degree of repeatability, whereas the data near the edge of the base ($R/R_B = 0.8$) are less consistent among the four flights. For $M_\infty < 4$ to 5, approximately, all data exhibit sharp increases with decreasing Mach number.[5] Also, the discontinuity[6] in p_b/p_∞ near $M_\infty = 1$ is clearly identifiable in the present results (Figs. 1 and 2). Although the Mach number trends exhibited by these data are typical of slender cones in general, the specific pressure levels correspond to ablating heatshields with $\dot{m}/\rho_\infty V_\infty A_B < 0.001$.

Data Correlation

An analysis was conducted to characterize the data using local flow parameters on the forebody immediately preceding the base. Base pressure measurements are correlated in Fig. 3. The local (turbulent boundary-layer edge) Mach number and static pressure on the cone were computed[7] in equilibrium air

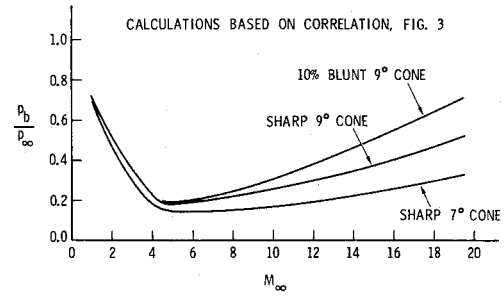

Fig. 4 Base pressure predictions for several slender cones ($\dot{m}/\rho_\infty V_\infty A_B < 0.001$).

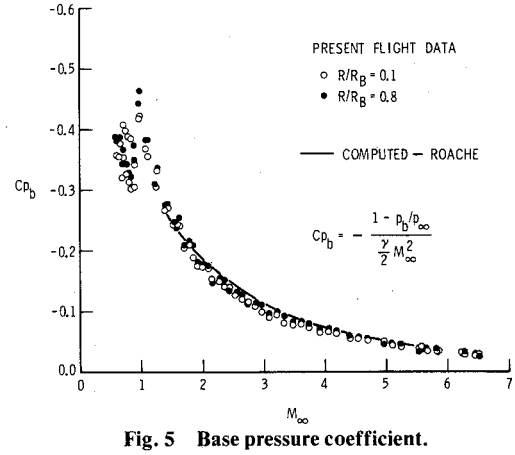

Fig. 5 Base pressure coefficient.

for the RV configurations and trajectories. This data compilation assumes the premise that a correlation based on local flow properties is appropriate for a wide variety of spherically blunted, conical configurations.[8] The utility of Fig. 3 is that from this single $p_b/p_c - M_c$ correlation a series of $p_b/p_\infty - M_\infty$ plots may be generated for flat-based RVs having various sphere-cone geometry, with $\dot{m}/\rho_\infty V_\infty A_B < 0.001$ as a special case.

Results

Forebody Configuration Effects

A number of slender configurations was chosen to assess the sensitivity of base pressure to nose bluntness (R_N/R_B) and cone angle (θ_c) variations for heatshields with very low mass addition characteristics. Typical calculations for several slender cones are illustrated in Fig. 4, based on the correlation of Fig. 3 in conjunction with Ref. 7. These results confirm, for the particular case $\dot{m}/\rho_\infty V_\infty A_B < 0.001$, that increasing either nose bluntness or cone angle tends to produce increases in the base pressure.[8]

Base Drag

The present flight-data measurements are replotted in Fig. 5 for $M_\infty < 7$ as the pressure coefficient for comparison with numerical solutions[1] for a 9° cone. Note that for most applications, the base drag coefficient will be determined from $C_{Db} = -Cp_b$. The data and computed results (limited to supersonic flow $M_\infty = 1.5$-5) are in excellent agreement. The flight data indicate a maximum C_{Db} of 0.46 near sonic speeds, and for slight reductions in Mach number below $M_\infty = 1$, the drag decreases abruptly (p_b/p_∞ increases).[9] Measured base drag coefficients in subsonic flow range from approximately 0.3 to 0.4 for Mach numbers greater than 0.5.

Conclusions

Flight-base pressure data obtained from slender conical reentry vehicles were correlated for the particular case of very

low heatshield ablation rates in turbulent flow. Effects of Mach number on base pressure in the hypersonic, supersonic, and subsonic flight regimes were emphasized. Results of the present analysis revealed that the base pressure increases with increasing nose bluntness and cone angle, in agreement with previous correlations of nonablating data. The derived base drag coefficient increases with decreasing Mach number in supersonic flow and exhibits a maximum value near sonic conditions; a pronounced decrease in drag (increased base pressure) occurs as the Mach number is reduced slightly below unity.

References

[1]Roache, P.J., "Base Drag Calculations in Supersonic Turbulent Axisymmetric Flows," *Journal of Spacecraft and Rockets,* Vol. 10, April 1973, pp. 285-287.

[2]Bulmer, B.M., "Flight Test Correlation Technique for Turbulent Base Heat Transfer with Low Ablation," *Journal of Spacecraft and Rockets,* Vol. 10, March 1973, pp. 222-224.

[3]Zarin, N.A., "Base Pressure Measurements on Sharp and Blunt 9°Cones at Mach Numbers from 3.50 to 9.20," *AIAA Journal,* Vol. 4, April 1966, pp. 743-745.

[4]Cassanto, J.M., "Flight Test Base Pressure Results at Hypersonic Mach Numbers in Turbulent Flow," *AIAA Journal,* Vol. 10, March 1972, pp. 329-331.

[5]Whitfield, J.D. and Potter, J.L., "On Base Pressures at High Reynolds Numbers and Hypersonic Mach Numbers," Arnold Engineering Development Center, Tullahoma, Tenn., AEDC-TN-60-61, March 1960.

[6]Cassanto, J.M., "A Base Pressure Experiment for Determining the Atmospheric Pressure Profile of Planets," *Journal of Spacecraft and Rockets,* Vol. 10, April 1973, pp. 253-261.

[7]Hochrein, G.J., "A Procedure for Computing Aerodynamic Heating on Sphere Cones," Sandia Labs., Albuquerque, N.M., SC-DR-69-449, Nov. 1969.

[8]Cassanto, J.M., "Effect of Cone Angle and Bluntness Ratio on Base Pressure," *AIAA Journal,* Vol. 3, Dec. 1965, pp. 2351-2352.

[9]Starr, R.F. and Varner, M.O., "Experimental and Theoretical Observations on the Drag of Bodies of Revolution at Transonic Speeds," AIAA Paper 76-90, Washington, D.C., 1976.

Displacement Field in the Nonlinear Theory of Shells

M. S. El Naschie*
Riyadh University, Saudia Arabia

THE present Note is concerned with a problem encountered in the definition of the displacement field for a cylindrical shell. Although the discussion is confined to cylindrical shells, it bears a somewhat fundamental character.

I. Using a convective coordinate system,[1] the Lagrangian strain tensor is defined as[1]

$$\gamma_{\alpha\beta} = \tfrac{1}{2}(\bar{g}_{\alpha\beta} - g_{\alpha\beta}) \tag{1}$$

where α and β are indices of the shell surface and $\bar{g}$, g are the metric tensors of the deformed and the undeformed systems, respectively. Further, the relationship between the physical strain components and the strain tensor is given by

$$\varepsilon_{(\alpha)} = \left(1 + 2\frac{\gamma_{\alpha\alpha}}{g_{\alpha\alpha}} - 1\right)^{1/2} \tag{2}$$

In order to expand this expression in a power series, we have to assume that

$$\left|\frac{\gamma_{\alpha\alpha}}{g_{\alpha\alpha}}\right| \leq \frac{1}{2} \tag{3}$$

Thus,

$$\varepsilon_{(\alpha)} = \frac{\gamma_{\alpha\alpha}}{g_{\alpha\alpha}} - \frac{1}{2}\left(\frac{\gamma_{\alpha\alpha}}{g_{\alpha\alpha}}\right)^2 + \frac{1}{2}\left(\frac{\gamma_{\alpha\alpha}}{g_{\alpha\alpha}}\right)^3 \tag{4}$$

II. The Lagrangian strain tensor can be expressed in terms of the displacement vector using a body fixed coordinate system. Let this be transformed into a cylindrical coordinate system (r, φ, S). Assuming the validity of the Love-Kirchhoff assumptions we have

$$\gamma_{z\varphi} = \gamma_{xz} = 0 \tag{5}$$

$$\varepsilon_{zz} = 0 \tag{6}$$

and

$$\mathfrak{W}(z) = \mathfrak{W}(0) + z/r[d\mathfrak{W}(0)/d(z/r)] \tag{7}$$

where $\mathfrak{W}(z=0)$ is the displacement vector of a generic point on a distance $z=0$ of the middle surface. For the sake of simplicity and clarity, we will write the $\gamma_{\varphi\varphi}$ component only. However, the results are easily generalized. In Cartesian coordinates† we have

$$\gamma_{yy}\Big|_{u=0} = dv/dy + \frac{1}{2}[(dv/dy)^2 + (dw/dy)^2] \tag{8}$$

and transformed into cylindrical coordinates we obtain

$$\gamma_{\varphi\varphi}\Big|_{u=0} = (\dot{v} + w)\frac{1}{r} + \frac{1}{2r^2}[(w + \dot{v})^2 + (\dot{w} - v)^2] \tag{9}$$

where w and v are the displacement components of a generic point P of the middle surface of a cylindrical shell and $(\dot{}) = (\,)/d\varphi$.

It should be emphasized that in deriving this nonlinear expression, no assumption has been made on the magnitude of the displacement. The sole restriction on $\gamma_{\varphi\varphi}$ is that the strain should be very small.

III. We now look at the two well-known possible definitions of the displacement components (w,v) describing the deformation of the point P, see Fig. 1. One definition is made possible by postulating that the point first moves a radial distance w towards the center of the undeformed cylinder, then sideways another distance v which is perpendicular to w, and thus tangential to the undeformed reference surface at the point P. Thus, the exact geometrical expression connecting the displacement components with the physical strain defined by

$$\varepsilon_\varphi = (d\bar{S}_\varphi - dS_\varphi)/dS_\varphi \tag{10}$$

is

$$\varepsilon_\varphi = \left[1 + \frac{1}{2}\left\{\frac{4}{r}(w + \dot{v}) + 2\left(\frac{\dot{v} + w}{r}\right)^2 + 2\left(\frac{\dot{w} - v}{r}\right)^2\right\}\right]^{1/2} - 1 \tag{11}$$

If the second term in brackets is defined as

$$\varepsilon_\varphi = [1 + \vartheta(w;v)]^{1/2} - 1 \tag{12}$$

Received May 13, 1975; revision received January 19, 1976.
Index category: Structural Stability Analysis.

*Research Associate, Department of Civil Engineering, University College, London, England. Member AIAA. Presently assisting professor in Riyadh University.

†See, for instance, V.V. Novozhilov, *Foundation of the Nonlinea Theory of Elasticity,* Graylock Press, pp. 4-15 and Eq. (1.22).